Acta Oncologica, 2015; 54: 224–231

informa
healthcare

ORIGINAL ARTICLE

Quantification of delineation errors of the gross tumor volume on magnetic resonance imaging in uterine cervical cancer using pathology data and deformation correction

AGUSTINUS J. A. J. VAN DE SCHOOT[1], PETER DE BOER[1], MARRIJE R. BUIST[2], JAAP STOKER[3], MAAIKE C. G. BLEEKER[4], LUKAS J. A. STALPERS[1], COEN R. N. RASCH[1] & ARJAN BEL[1]

[1]*Department of Radiation Oncology, Academic Medical Center, University of Amsterdam, Amsterdam, The Netherlands,* [2]*Department of Gynecologic Oncology, Academic Medical Center, University of Amsterdam, Amsterdam, The Netherlands,* [3]*Department of Radiology, Academic Medical Center, University of Amsterdam, Amsterdam, The Netherlands and* [4]*Department of Pathology, Academic Medical Center, University of Amsterdam, Amsterdam, The Netherlands*

ABSTRACT

Background. To safely optimize target volumes using magnetic resonance imaging (MRI) for uterine cervical cancer radiation therapy, MRI findings need to be validated. The aim of this study was to correlate pre-operatively acquired MRI and surgical specimen imaging for uterine cervical cancer patients using deformable image registration and quantify gross tumor volume (GTV) delineation discrepancies.

Material and methods. For 16 retrospectively selected early-stage uterine cervical cancer patients, the cervix-uterus structure, uterine cavity and the GTV were delineated on 2D pathology photos after macroscopic intersection and corresponding pre-operatively acquired T2-weighted 2D sagittal MR images. Segmentations of pathology photos and MR images were simultaneously registered using a three-step multi-image registration strategy. The registration outcome was evaluated by the Dice similarity coefficient (DSC) and the surface distance error (SDE). In addition, GTV expansions within the cervix-uterus structure needed to obtain 95% GTV coverage were determined.

Results. After three-step multi-image registration, the median DSC and median SDE were 0.98 and 0.4 mm (cervix-uterus) and 0.90 and 0.4 mm (uterine cavity), respectively. The average SDE around the GTV was 0.7 mm (range, 0.1 mm – 2.6 mm). An underestimation of MRI-based GTV delineations was found when no margin was applied, indicated by a mean GTV coverage of 61%. To obtain 95% GTV coverage for 90% of the patients, a minimum 12.0 mm margin around MRI-based GTVs was needed.

Conclusion. The presented three-step multi-image registration strategy was suitable and accurate to correlate MRI and pathology data for uterine cervical cancer patients. To cover the pathology-based GTV, a margin of at least 12.0 mm around GTV delineations on T2-weighted MRI is needed.

The treatment policy in patients with uterine cervical cancer is mainly based on the stage of the tumor, indicated by the International Federation of Gynecology and Obstetrics (FIGO) staging system. Surgery is usually recommended for patients with early-stage uterine cervical cancer (FIGO stage IB–IIA). Radiation therapy (RT) with concurrent chemotherapy is the cornerstone of treatment for patients with locally advanced uterine cervical cancer (FIGO stage IIB–IVA) [1,2].

According to clinical guidelines for RT treatment of uterine cervical cancer, the clinical target volume (CTV) is defined as the gross tumor volume (GTV) together with the entire uterine cervix and body [3,4]. The planning target volume (PTV) is obtained by adding an additional margin around the CTV to account

Correspondence: A. J. A. J. van de Schoot, Department of Radiation Oncology, Academic Medical Center, University of Amsterdam, Meibergdreef 9, 1105 AZ, Amsterdam, The Netherlands. Tel: + 31 205664231. Fax: + 31 206091278. E-mail: a.j.schootvande@amc.uva.nl

(Received 20 August 2014; accepted 29 October 2014)

ISSN 0284-186X print/ISSN 1651-226X online © 2014 Informa Healthcare
DOI: 10.3109/0284186X.2014.983655

for uncertainties, such as uncertainties in daily set-up, delineation and organ motion [5–8]. Despite the limited local recurrence rate after RT, large treatment volumes cause serious late vaginal, bowel and bladder toxicity, which significantly reduces quality of life [2].

To substantially decrease the target volume and spare healthy tissue during uterine cervical cancer RT, it has been suggested to only include the invaded part of the uterine body in the CTV [9,10]. However, information of the exact tumor extent is necessary in order to optimize treatment volumes in uterine cervical cancer RT. Since the GTV is poorly visible on computed tomography (CT) images acquired for RT treatment planning [11–13], distinction between tumor and healthy tissue on CT is not reliable. Therefore, magnetic resonance imaging (MRI) is considered as an additional imaging modality for RT treatment planning to assess the exact tumor extent [14]. However, the accuracy of tumor delineation on MRI needs to be validated by comparing tumor extent visible on MRI with the corresponding pathology-proven tumor extension [10].

Previously, several studies have been performed to correlate MRI and pathology data in order to validate MRI findings. The majority of those reported studies were performed on the prostate gland, e.g. [15,16], but also a few studies on other organs were reported, e.g. [17]. For uterine cervical cancer imaging data, only a limited number of studies addressed the validation of MRI findings [18,19]. However, in none of these studies the potentially large deformation between the in vivo structure on MRI and pathology specimen after surgical removal was corrected. In this study, pathology imaging will be used to validate GTV delineations on MRI using deformable image registration in uterine cervical cancer patients.

The aim of this study was to develop a method to correlate pre-operatively acquired MRI and surgical specimen imaging for early-stage uterine cervical cancer patients, including corrections for potential large shape deformations. In addition, the discrepancy between MRI-based and pathology-based GTV delineations after deformable image registration was quantified.

Material and methods

Patient data

According to clinical guidelines, uterine cervical cancer patients who received a radical hysterectomy with pelvic lymphadenectomy underwent anatomical MRI prior to surgery. The standard MRI protocol consisted of sagittal, axial oblique and coronal oblique T2-weighted turbo spin-echo sequences (repetition time/echo time = 2500/70 ms, field of view 300×300 mm^2, acquisition matrix 512×384, slice thickness 4.0 mm and turbo factor 11) in supine position on a 1.5 Tesla whole-body MRI system (Siemens Avanto, Erlangen, Germany). After surgery, the pathologist routinely analyzed the fresh surgical specimen by making an anterior median incision to expose the internal os of the uterus. A digital photo of this macroscopic intersection was only made if the remaining tumor was still visible macroscopically after pre-operatively performed biopsies.

Patients who received a radical hysterectomy for cervical carcinoma between January 2012 and December 2013 were selected retrospectively based on the availability of pre-operative MRI data and a digital photo of the surgical specimen obtained during pathology analysis. After exclusion of three patients [GTV invisibility on either MRI or digital photo (2), presence of a large uterine fibroid (1)], 16 uterine cervical cancer patients with FIGO stages IB1 (10), IB2 (5) and IIA1 (1) were included with MRI acquired on average 24 days prior to surgery (range, 14–48 days). The pathology photos and the sagittal T2-weighted MRI data corresponding to the plane of the anterior median incision were used to correlate pathology findings with pre-operatively acquired MRI data.

Delineation and segmentation

For each patient, two radiation oncologists independently delineated the cervix-uterus structure, i.e. uterus including the uterine cervix, the uterine cavity and the GTV, i.e. the macroscopically visible tumor extension, on the sagittal T2-weighted MRI (Figure 1b) according to clinical guidelines [3,4]. Also, for GTV delineation on MRI, access to the radiology report was available. With at least one week in between, one of these two radiation oncologists also delineated corresponding structures (cervix-uterus, uterine cavity and GTV) on all anonymized pathology photos. To obtain reliable and accurate pathology-based delineations and avoid bias, delineations on pathology photos were created independently without information of previously performed delineations and subsequently revised by an experienced pathologist (Figure 1a).

The mid-sagittal 2D MR image, representing the central part of the uterine body and corresponding to the plane of macroscopic intersection, was selected based on uterine cavity visibility. Since the uterine cavity is located in the central part of the uterine body, it was only visible in a limited number of sagittal 2D MR images; therefore, the uterine cavity was considered a reliable landmark for corresponding image selection. After selection, the delineated structures were segmented from the background on pathology photos and from surrounding tissue on corresponding MR images (Figure 1c and d). Also,

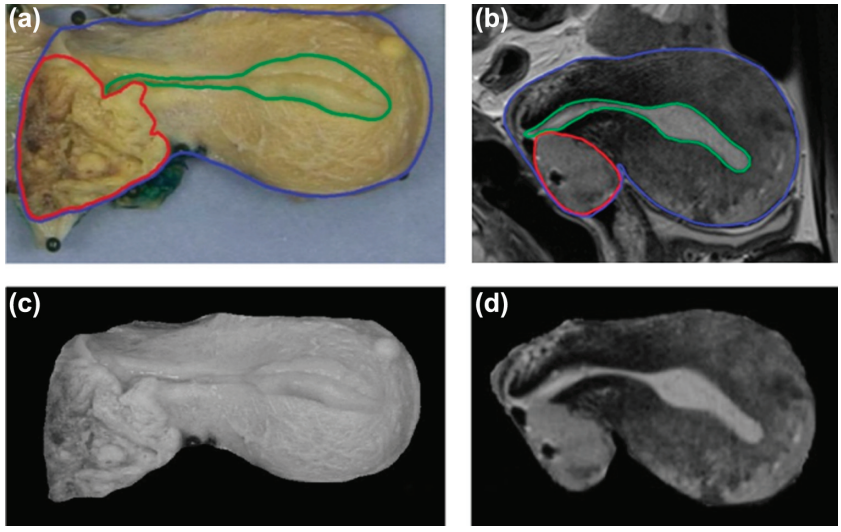

Figure 1. An example of a 2D digital photo of the macroscopic intersection (a) and the corresponding 2D sagittal MR image (b) with delineated structures [cervix-uterus (blue), uterine cavity (green), GTV (red)]. The cervix-uterus structures were segmented from the background on the photo (c) and from surrounding tissue on MRI (d).

all segmented grayscale images were transformed to binary images with pixel values inside the structures set to true and those outside the structures set to false (Supplementary Figure A1, to be found online at http://informahealthcare.com/doi/abs/10.3109/0284186X.2014.983655).

MRI-pathology registration

Pathology data were registered to MRI data based on a three-step multi-image registration strategy using Elastix, a freely available image registration software package [20]. First, a rigid registration was performed between binary image pairs of the cervix-uterus based on translations and rotations. Next, affine multi-image registration was achieved using a weighted contribution of binary image pairs of the cervix-uterus and the uterine cavity based on translation, rotation, scaling and shearing. To finalize the three-step registration strategy and correct for deformations, a B-splines based deformable multi-image registration step was performed using a weighted contribution of segmented grayscale image pairs of the cervix-uterus and the uterine cavity (Supplementary Figure A2, to be found online at http://informahealthcare.com/doi/abs/10.3109/0284186X.2014.983655). The transformation ($\boldsymbol{T}$) between the pathology photo (I_{PAT}) and its corresponding MR image (I_{MRI}) using a multi-image registration process with a weighted contribution was determined by optimizing the registration cost function ($\boldsymbol{C}$) of multiple image pairs with its associated weight factor (ω_i) (Equation 1).

$$\boldsymbol{C}(\boldsymbol{T}; I_{MRI}, I_{PAT}) = \frac{1}{\sum_{i=1}^{N} \omega_i} \sum_{i=1}^{N} \omega_i \boldsymbol{C}(\boldsymbol{T}; I^i_{MRI}, I^i_{PAT}) \quad (1)$$

Optimal contributions of the cervix-uterus image pair (ω_{CU}) and the uterine cavity image pair (ω_{UCa}) to the final registration result were determined for each patient (Supplementary Figure B1 and B2, to be found online at http://informahealthcare.com/doi/abs/10.3109/0284186X.2014.983655). An equal contribution of both image pairs ($\omega_{CU} = 0.5$; $\omega_{UCa} = 0.5$) was used in nine patients and a larger (smaller) contribution of the cervix-uterus image pair compared to the uterine cavity image pair was used in three (four) patients. For each registration step, image registration was performed using B-spline interpolation, multi-resolution registration, normalized mutual information similarity measure and gradient descent optimization. The three-step multi-image registration process was performed twice with segmented MR images based on delineations of each radiation oncologist (REG_1 and REG_2).

Registration evaluation

Given the delineations of both radiation oncologists on MRI, the inter-observer delineation variation was quantified by calculating the conformity index (CI). The CI was defined as the ratio of the overlapping and the encompassing delineated volumes and chosen as conformity metric to enable a comparison with published data [21]. After three-step multi-image registration, the registration result was first inspected visually by displaying the MR image together with the deformed pathology photo. Next, the outcome of image registration was evaluated by determination of the surface distance error (SDE) and the Dice similarity coefficient (DSC) [22] for both the cervix-uterus and the uterine cavity structure. Also, the SDE

of the boundary points from the cervix-uterus structure around the GTV, the GTV-S, was calculated.

The SDE described the registration error and was defined as the mean of all minimum distances between boundary points of the reference structure and the corresponding deformed structure. The DSC is frequently used to describe the overlap between corresponding structures [20,22] and was defined as the number of pixels shared by the structure on MRI (PIX_{MRI}) and the structure on the pathology photo (PIX_{PATH}) divided by the average amount of pixels in both structures (Equation 2).

$$DSC = 2\frac{PIX_{MRI} \cap PIX_{PATH}}{PIX_{MRI} + PIX_{PATH}} \quad (2)$$

Absolute pixel displacements, differences between pixel displacement vectors after the second and third registration step, were evaluated in order to indicate possible unrealistic displacements within the different structures. The improvement of registration accuracy was studied by testing (Wilcoxon signed-rank test) the difference in registration accuracy (DSC and SDE) obtained after each registration step for both the cervix-uterus and the uterine cavity. Moreover, the robustness of our proposed registration strategy was determined by calculating the registration accuracy for both the cervix-uterus and the uterine cavity using the sagittal T2-weighted MR images adjacent to the corresponding MR image during three-step multi-image registration for REG_1.

GTV validation

Pathology-based GTV delineations, denoted as the reference GTV (GTV_{REF}), were used to validate T2-weighted MRI-based GTV delineations (GTV_{MRI}). The GTV_{REF} was deformed according to the obtained transformation after three-step multi-image registration and the coverage of the deformed GTV_{REF} with the GTV_{MRI} was calculated (Equation 3).

$$GTVcoverage = \frac{GTV_{MRI} \cap GTV_{REF}}{GTV_{REF}} \times 100\% \quad (3)$$

Margins needed around MRI-based GTV delineations to obtain 95% GTV coverage for at least 90% of the patients were determined by uniformly expanding the GTV_{MRI} using a 2.0 mm step size. The expansions were performed only within the cervix-uterus structure to mainly represent the GTV discrepancy along the axis of the uterine body (Supplementary Figure C1, to be found online at http://informahealthcare.com/doi/abs/10.3109/0284186X.2014.983655). For each applied margin, the coverage of the GTV_{REF} with the expanded GTV_{MRI} was calculated. To investigate the effect of inter-observer variation on obtained margins, coverage based on the GTV_{MRI} from the first and the second radiation oncologist ($GTV_{MRI\text{-}1}$ and $GTV_{MRI\text{-}2}$, respectively) was determined.

After margin determination needed to obtain 95% GTV coverage, correlations with the observed time interval between MRI and surgery and with the GTV_{MRI} were tested [Pearson's correlation coefficient (R)]. To investigate the influence of deformable image registration in terms of GTV coverage, we also determined GTV coverage based on image registration results after only rigid registration.

Results

A limited inter-observer delineation variation on MRI was observed, indicated by a median CI of 0.88, 0.63 and 0.80 for the cervix-uterus, uterine cavity and GTV, respectively. Box-and-whisker plots present the registration accuracy after REG_1. The multi-image deformable registration step improved the correlation between the cervix-uterus as well as the uterine cavity significantly ($p < 0.01$), indicated by the increased median DSC and decreased median SDE (Figure 2a and b). Similar registration accuracy was obtained after REG_2 (Supplementary Figure D1, to be found online at http://informahealthcare.com/doi/abs/10.3109/0284186X.2014.983655). Also, the small inter-observer delineation variation led to similar mean GTV-S registration errors of 0.7 mm (range, 0.2 mm – 2.6 mm) and 0.6 mm (range, 0.1 mm – 2.0 mm) after REG_1 and REG_2, respectively. Supplementary Figure A2 (to be found online at http://informahealthcare.com/doi/abs/10.3109/0284186X.2014.983655) shows a typical example of segmented grayscale images after three-step multi-image registration.

Overall pixel displacements caused by multi-image deformable registration inside the GTV (4.8 mm, 6.0 mm) were similar to displacements inside the cervix-uterus (5.5 mm, 7.0 mm) and the uterine cavity (4.7 mm, 6.3 mm) for REG_1 and REG_2, respectively. Also, similar displacements inside defined structures after REG_1 and REG_2 were found without unrealistic pixel displacements (Supplementary Table E1, to be found online at http://informahealthcare.com/doi/abs/10.3109/0284186X.2014.983655). Robustness evaluation showed similar cervix-uterus registration accuracy using adjacent MR images instead of corresponding MR images (Figure 2c and d). However, larger registration errors for internal structures were obtained when using adjacent MR images.

After three-step multi-image registrations, an underestimation of GTV_{MRI} compared to the GTV_{REF} was determined when no margin was applied, indicated by a median GTV coverage of 59% (range, 43–95%) for

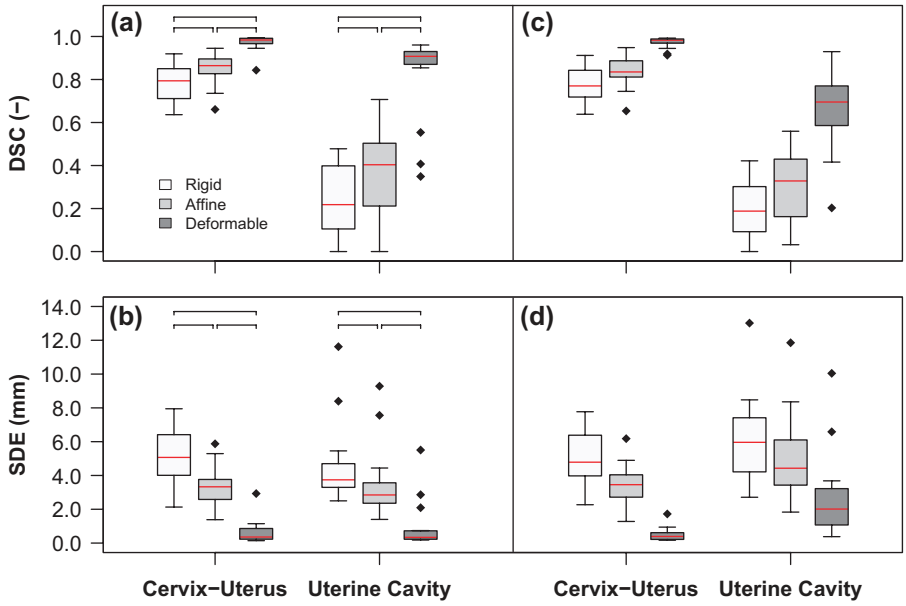

Figure 2. Box-and-whisker plots of the DSC and the SDE between the MR image and the pathology photo (a, b) and between adjacent MR images and the pathology photo (c, d) after each step in the three-step multi-image registration strategy (rigid registration, affine registration and deformable registration) for the cervix-uterus and the uterine cavity structure. The box represents the upper and lower quartiles (IQR) and the band (red) inside the box the median value. The whisker represents the highest (lowest) value within 1.5 IQR of the upper (lower) quartile. Dots above or below the whiskers are considered outliers. Horizontal lines indicate statistical significant difference ($p < 0.01$).

GTV_{MRI-1} after REG_1 and 57% (range, 11% – 98%) for GTV_{MRI-2} after REG_2 (Figure 3). To acquire a median GTV coverage of 95%, expansions of the GTV_{MRI} within the cervix-uterus structure of 6.0 mm and 8.0 mm were needed for GTV_{MRI-1} and GTV_{MRI-2}, respectively. Furthermore, 95% GTV coverage for 90% of the patients was obtained using margins around the GTV_{MRI} of 12.0 mm (REG_1, GTV_{MRI-1}) and 18.0 mm (REG_2, GTV_{MRI-2}) and 100% GTV coverage for all patients was acquired using a 22.0 mm margin around the GTV_{MRI} in both cases. Determination of GTV coverage using GTV_{MRI-1} (GTV_{MRI-2}) after REG_2 (REG_1) provided similar results (Supplementary Figure F1, to be found online at http://informahealthcare.com/doi/abs/10.3109/0284186X.2014.983655). However, neither of all expansions included a margin uncertainty

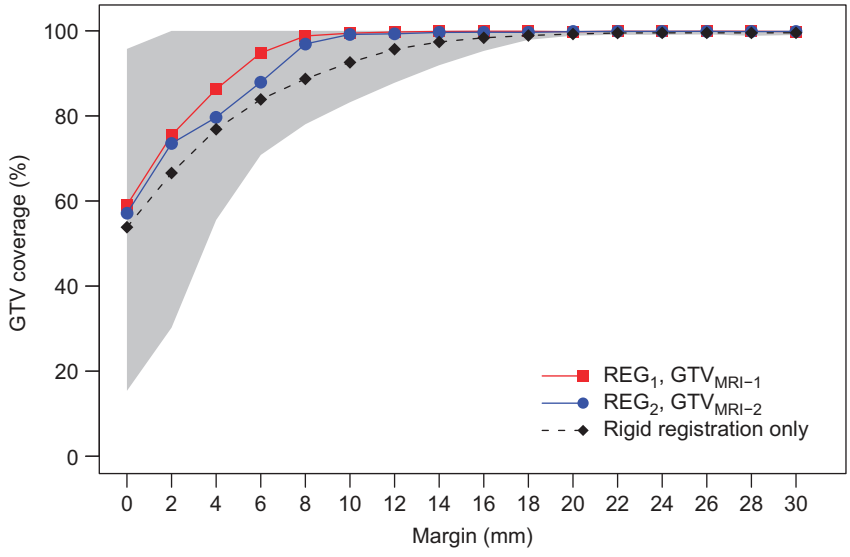

Figure 3. Median GTV coverage after three-step multi-image registration based on GTV_{MRI-1} after REG_1 (red squares) and based on GTV_{MRI-2} after REG_2 (blue circles) as a function of applied margin to the GTV_{MRI} within the cervix-uterus structure. The black dashed line shows the average median GTV coverage of both observations after only rigid registration and the gray region indicates the 95% confidence interval of both observations after three-step multi-image registration.

induced by the registration error of 1.0 mm. For the margins needed to obtain 95% GTV coverage, no significant correlation were found with time interval between MRI and surgery ($R = 0.21$, $p = 0.24$) and with GTV size ($R = 0.15$, $p = 0.40$).

Without deformation correction, i.e. after rigid registration for REG_1 and REG_2, an average median GTV coverage of 54% was found when no margin was applied. Compared to the results after deformation correction, a larger margin (12.0 mm) was needed to obtain a median GTV coverage of 95% (Figure 3). Moreover, image alignment based on only translations and rotations led to a larger registration error (about 4.0 mm) which induced an additional uncertainty on top of the determined margin to obtain GTV coverage.

Discussion

This study described a novel method to correlate preoperatively acquired MRI and surgical specimen imaging for uterine cervical cancer patients, including large deformation corrections. Our proposed three-step multi-image registration strategy is based on boundary and internal structures and accurate correlations between MRI and pathology photos were obtained. Moreover, we corrected for possible large deformations between in vivo and ex vivo organ shapes by using deformable multi-image registration. In addition, the discrepancy between GTV delineations on T2-weighted MRI and pathology imaging after deformable registration was quantified by the coverage of GTV_{REF} with GTV_{MRI}. To obtain 95% GTV coverage for at least 90% of the patients, a margin of at least 12.0 mm around the GTV_{MRI} was needed. We have shown that correlations between MRI and pathology data could be obtained by deformable image registration and used for GTV validation.

Unlike methods in previously reported studies on MRI and pathology correlation for uterine cervical cancer patients [11,18], our correlation method corrected for shape deformations between both imaging data sets and therefore made the validation of GTV delineations more reliable. Without deformation corrections, less accurate correlations between MRI and pathology data were obtained and a larger margin around GTV delineations on MRI would be needed to safely cover the pathology-based GTV. Consequently, our three-step multi-image registration led to a more accurate validation of MRI-based GTV delineations compared to only rigid alignment. Moreover, the GTV_{MRI} including the margin to correct for pathology-proven macroscopic tumor extensions can be used to better define RT volumes when only the invaded part of the uterine body will be included.

Besides the boundary contour, the only corresponding landmark that could be clearly distinguished on both imaging data sets was the uterine cavity structure. To avoid registration outcome largely driven by the segmented boundary contour, a multi-image registration strategy was defined using grayscale images to also align internal structures. Using only segmented images based on boundary contours or internal structures for image registration led to a worse registration outcome compared to our method (Supplementary Figure B1 and B2, to be found online at http://informahealthcare.com/doi/abs/10.3109/0284186X.2014.983655). As a consequence, registration evaluation based on structures that were not used to optimize the registration could not be performed and registration-independent corresponding landmarks were unavailable. Therefore, registration evaluation was performed based on the cervix-uterus and the uterine cavity structures, assuming these structures represented the correlation of the entire specimen. Additionally, the GTV-S structure was defined to analyze the registration error around the GTV.

The advantage of our registration method is the use of multiple imaging pairs to optimize the final transformation using both boundary and internal structure information. Since no previous studies reported on optimized image contributions during multi-image registration, a patient-specific image pair contribution was used. Based on all patient-specific contributions, we also determined a population-based image pair contribution which can be used for ensuing patients.

This study has some limitations, mainly due to the retrospective character of this study. Only one 2D digital photo of the macroscopic intersection obtained during pathology analysis of the surgical specimen was available and we used this photo to correlate MRI and pathology data. Although 3D MRI data was available, 2D-3D image registration could not be performed reliably due to the absence of corresponding landmarks for guidance of the registration algorithm. Therefore corresponding 2D MR images were manually selected based on information of intersection directions during pathology analysis and uterine cavity visibility. Even though both images were assumed to be in the same plane, the exact direction of intersection during pathology analysis was unknown and possible rotations could have influenced the registration accuracy. Since a relatively small difference in the registration result was found due to corresponding image selection uncertainty, the impact on the determined margin was estimated to be limited and in the same order of magnitude as the difference in registration results.

Due to the absence of whole-mount sections, microscopic tumor spread could not be determined and the GTV_{MRI} was validated based on the macro-

scopically visible tumor on pathology photos. To safely optimize the CTV based on only the GTV_{MRI}, a future study using 3D data sets and whole-mount sections will be needed to decrease uncertainties and improve correlations in other directions (transverse, coronal). Nevertheless, the tumor extension along the axis of the uterine body is of most interest and quantification of this extension might enable a safe exclusion of the healthy part of the uterine body from RT treatment volumes. Since GTV_{MRI} expansions were performed uniformly but only within the cervix-uterus structure, the obtained margins represented discrepancies between MRI-based GTV delineations and pathology-proven GTV coverage along the axis of the uterine body.

Only anatomical T2-weighted MRI was available, because MRI was only intended to be used to determine the stage, size and location of the tumor prior to surgery. To better define the GTV and to optimize target volumes for RT purposes, quantitative MRI such as diffusion-weighted imaging or dynamic contrast-enhanced MRI can offer additional valuable information [23]. These techniques can improve tumor detection, contribute to tumor differentiating or may predict treatment response.

Since this study was performed from a RT perspective, all structures on MRI were delineated by radiation oncologists as being common practice in clinical RT. The observed small inter-observer delineation variation on MRI was in agreement with previously reported results [21]. This small variation resulted in limited impact on MRI-pathology correlation and GTV_{MRI} validation and indicated a negligible delineation bias. If appropriate tools become available, delineations on MRI can be performed automatically to eliminate the inter-observer variation. According to present RT margin concepts [7], the GTV is defined as the macroscopically visible tumor on a specific imaging modality and GTV uncertainty corrections are included in the CTV-to-PTV margin. In this study, the proposed GTV_{MRI} margin is defined to obtain GTVs that approximate macroscopically visible tumors on pathology photos. However, this margin is not directly covered by the present margin concepts. Since target volume optimization using the GTV_{MRI} margin already included possible delineation uncertainties, a CTV-to-PTV margin without a component for delineation uncertainties is warranted.

All included patients had early-stage uterine cervical cancer (FIGO stage IB–IIA) and in general only patients with locally advanced uterine cervical cancer (FIGO stage IIB–IVA) will be treated with RT and concurrent chemotherapy. However, the validation of MRI findings using pathology data cannot be performed for patients with locally advanced tumors because these patients did not undergo surgery. Since digital photos of the median incision were only taken if the tumor was still visible macroscopically after the biopsies taken before surgery, early-stage uterine cervical cancer patients with relatively large tumors were included.

Despite the accurate observed correlations for the evaluated structures, discrepancies between GTV_{MRI} and GTV_{REF} were observed after three-step multi-image registrations. Although the exact reason for this discrepancy is unknown, it could be induced by a change in tumor size within the time between MRI acquisition and surgery due to practical workflow issues. However, the influence of this time interval on possible tumor growth is likely to be relatively small, as we found no significant correlation between observed time intervals and determined discrepancies. Furthermore, based on the observed time intervals and reported typical pre-treatment cervical tumor doubling times of 80–160 days [24] an average increase of 5% (range, 2% – 10%) in the radius of tumor volumes could be expected. Given this very limited possible increase in tumor volumes within the time between MRI acquisition and surgery together with the weak correlation between observed time intervals and determined discrepancies, the influence of the time interval on obtained margins was assumed to be negligible. In addition, previous studies on MRI-pathology correlation reported similar time intervals between imaging and surgery [11,18]. Besides due to the time interval, the GTV_{MRI} could be underestimated due to the use of only one standard MRI sequence [21] or the GTV_{REF} could be overestimated due to the retrospective determination of the macroscopically visible tumor. A future prospective study using a dedicated pathology analysis and different MRI sequences will decrease these uncertainties.

In conclusion, three-step multi-image registration including deformation corrections provided accurate correlations between pre-operatively acquired MRI and surgical specimen imaging for uterine cervical cancer patients. In addition, a margin of at least 12.0 mm around MRI-based GTV delineations is needed to cover the macroscopically visible tumor extension on surgical specimen imaging. A prospective study on MRI and pathology correlation may further improve tumor definition in order to optimize RT treatment volumes and reduce radiation-induced toxicity for uterine cervical cancer patients.

Declaration of interest: Dr Bel reports grants and non-financial support from Elekta, outside the submitted work; Dr Stoker reports grants from Robarts Clinical Trials, outside the submitted work. Elekta and Robarts Clinical Trials had no involvement in study design, data collection and analysis, and writing of the manuscript. The authors alone are responsible for the content and writing of the paper.

References

[1] Eifel PJ, Winter K, Morris M, Levenback C, Grigsby PW, Cooper J, et al. Pelvic irradiation with concurrent chemotherapy versus pelvic and para-aortic irradiation for high-risk cervical cancer: An update of radiation therapy oncology group trial (RTOG) 90-01. J Clin Oncol 2004;22:872–80.

[2] Vale CL, Tierney JF, Davidson SE, Drinkwater KJ, Symonds P. Substantial improvement in UK cervical cancer survival with chemoradiotherapy: Results of a royal college of radiologists' audit. Clin Oncol 2010;22:590–601.

[3] Haie-Meder C, Pötter R, van Limbergen E, Briot E, de Brabandere M, Dimopoulos J, et al. Recommendations from Gynaecological (GYN) GEC-ESTRO Working Group (I): Concepts and terms in 3D image based 3D treatment planning in cervix cancer brachytherapy with emphasis on MRI assessment of GTV and CTV. Radiother Oncol 2005;74:235–45.

[4] Tanderup K, Georg D, Pötter R, Kirisits C, Grau C, Lindegaard JC. Adaptive management of cervical cancer radiotherapy. Semin Radiat Oncol 2010;20:121–9.

[5] Tyagi N, Lewis JH, Yashar CM, Vo D, Jiang SB, Mundt AJ, et al. Daily online cone beam computed tomography to assess interfractional motion in patients with intact cervical cancer. Int J Radiat Oncol Biol Phys 2011;80:273–80.

[6] Haripotepornkul NH, Nath SK, Scanderbeg D, Saenz C, Yashar CM. Evaluation of intra- and inter-fraction movement of the cervix during intensity modulated radiation therapy. Radiother Oncol 2011;98:347–51.

[7] van Herk M. Errors and margins in radiotherapy. Semin Radiat Oncol 2004;14:52–64.

[8] Bondar ML, Hoogeman MS, Mens JW, Quint S, Ahmad R, Dhawtal G, et al. Individualized nonadaptive and online-adaptive intensity-modulated radiotherapy treatment strategies for cervical cancer patients based on pretreatment acquired variable bladder filling computed tomography scans. Int J Radiat Oncol Biol Phys 2012;83:1617–23.

[9] Lim K, Small W, Portelance L, Creutzberg C, Jürgenliemk-Schulz IM, Mundt A, et al. Consensus guidelines for delineation of clinical target volume for intensity-modulated pelvic radiotherapy for the definitive treatment of cervix cancer. Int J Radiat Oncol Biol Phys 2011;79:348–55.

[10] de Boer P, Adam JA, Buist MR, van de Vijver MJ, Rasch CR, Stoker J, et al. Role of MRI in detecting involvement of the uterine internal os in uterine cervical cancer: Systematic review of diagnostic test accuracy. Eur J Radiol 2013;82:e422–8.

[11] Mitchell DG, Snyder B, Coakley F, Reinhold C, Thomas G, Amendola M, et al. Early invasive cervical cancer: Tumor delineation by magnetic resonance imaging, computed tomography, and clinical examination, verified by pathologic results, in the ACRIN 6651/GOG 183 Intergroup Study. J Clin Oncol 2006;24:5687–94.

[12] Bipat S, Glas AS, van der Velden J, Zwinderman AH, Bossuyt PMM, Stoker J. Computed tomography and magnetic resonance imaging in staging of uterine cervical carcinoma: A systematic review. Gynecol Oncol 2003;91:59–66.

[13] Subak LL, Hricak H, Powell CB, Azizi L, Stern JL. Cervical carcinoma: Computed tomography and magnetic resonance imaging for preoperative staging. Obstet Gynecol 1995;86:43–50.

[14] Barillot I, Reynaud-Bougnoux A. The use of MRI in planning radiotherapy for gynaecological tumours. Cancer Imaging 2006;6:100–6.

[15] Park H, Piert MR, Khan A, Shah R, Hussain H, Siddiqui J, et al. Registration methodology for histological sections and in vivo imaging of human prostate. Acad Radiol 2008;15:1027–39.

[16] Groenendaal G, Moman MR, Korporaal JG, van Diest PJ, van Vulpen M, Philippens MEP, et al. Validation of functional imaging with pathology for tumor delineation in the prostate. Radiother Oncol 2010;94:145–50.

[17] Caldas-Magalhaes J, Kasperts N, Kooij N, van den Berg CAT, Terhaard CHJ, Raaijmakers CPJ, et al. Validation of imaging with pathology in laryngeal cancer: Accuracy of the registration methodology. Int J Radiat Oncol Biol Phys 2012;82:e289–98.

[18] deSouza NM, Scoones D, Krausz T, Gilderdale DJ, Soutter WP. High-resolution MR imaging of stage I cervical neoplasia with a dedicated transvaginal coil: MR features and correlation of imaging and pathologic findings. Am J Roentgenol 1996;166:553–9.

[19] Zhang Y, Hu J, Li J, Wang N, Li W, Zhou Y, et al. Comparison of imaging-based gross tumor volume and pathological volume determined by whole-mount serial sections in primary cervical cancer. Onco Targets Ther 2013;6:917–23.

[20] Klein S, Staring M, Murphy K, Viergever MA, Pluim JPW. Elastix: A toolbox for intensity-based medical image registration. IEEE Trans Med Imaging 2010;29:196–205.

[21] Dimopoulos JCA, de Vos V, Berger D, Petric P, Dumas I, Kirisits C, et al. Inter-observer comparison of target delineation for MRI-assisted cervical cancer brachytherapy: Application of the GYN GEC-ESTRO recommendations. Radiother Oncol 2009;91:166–72.

[22] Mazaheri Y, Bokacheva L, Kroon D-J, Akin O, Hricak H, Chamudot D, et al. Semi-automatic deformable registration of prostate MR images to pathological slices. J Magn Reson Imaging 2010;32:1149–57.

[23] Sala E, Rockall A, Rangarajan D, Kubik-Huch RA. The role of dynamic contrast-enhanced and diffusion weighted magnetic resonance imaging in the female pelvis. Eur J Radiol 2010;76:367–85.

[24] Wyatt RM, Beddoe AH, Dale RG. The effects of delays in radiotherapy treatment on tumour control. Phys Med Biol 2003;48:139–55.

Supplementary material available online

Supplementary Figures A1 and A2, Details on weight factor optimization, including Supplementary Figures B1 and B2, Supplementary Figure C1, D1, Table E1 and Figure F1 to be found online at http://informahealthcare.com/doi/abs/10.3109/0284186X.2014.983655